

RESEARCH ARTICLE | NOVEMBER 26 2024

Wave steepening and shock formation in ultracold neutral plasmas

M. K. Warrens  ; N. Plnman  ; G. M. Gorman  ; B. THusick  ; S. J. Bradshaw  ; T. C. Killian 

 Check for updates

Phys. Plasmas 31, 113503 (2024)
<https://doi.org/10.1063/5.0237455>

 CHORUS

 View
Online

 Export
Citation

Articles You May Be Interested In

Experimental and computational study of phase space dynamics in strongly coupled plasmas with steep density gradients

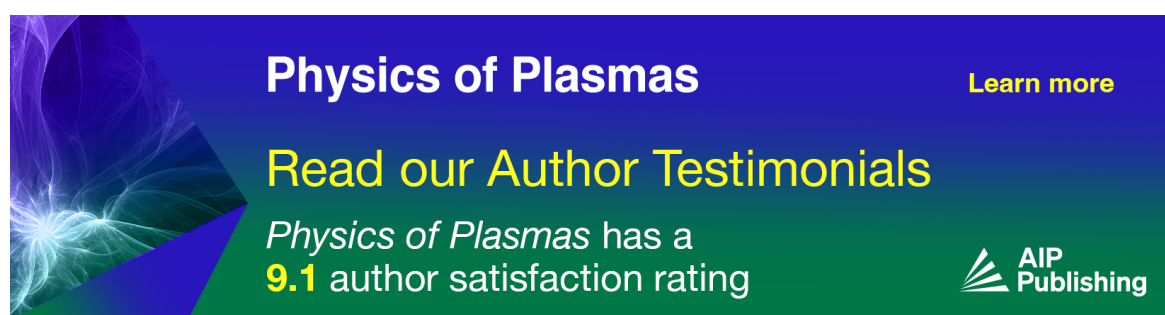
Phys. Plasmas (March 2025)

Computational investigation of wave steepening in a two-dimensional duct

J. Acoust. Soc. Am. (November 2000)

Spherical steepened wave in interstellar van der Waals dusty gas clouds

Physics of Fluids (August 2024)



Physics of Plasmas [Learn more](#)

Read our Author Testimonials

Physics of Plasmas has a **9.1** author satisfaction rating

 AIP Publishing

Wave steepening and shock formation in ultracold neutral plasmas

Cite as: Phys. Plasmas 31, 113503 (2024); doi: 10.1063/5.0237455

Submitted: 5 September 2024 · Accepted: 1 November 2024 ·

Published Online: 26 November 2024



View Online



Export Citation



CrossMark

M. K. Warrens,¹  N. P. Inman,^{1,a)}  G. M. Gorman,²  B. T. Husick,¹  S. J. Bradshaw,¹  and T. C. Killian¹ 

AFFILIATIONS

¹Rice University, 6100 Main St. Houston, Houston, Texas 77005, USA

²Sandia National Laboratories, 1515 Eubank Blvd SE, Albuquerque, New Mexico 87185, USA

^{a)}Author to whom correspondence should be addressed: npi1@rice.edu

ABSTRACT

We present observations of wave steepening and signatures of shock formation during expansion of ultracold neutral plasmas formed with an initial density distribution that is centrally peaked and decays exponentially with distance. The plasma acceleration and velocity decrease at large distance from the plasma center, leading to central ions overtaking ions in the outer regions and the development of a steepening front that is narrow compared to the size of the plasma. The density and velocity change dramatically across the front, and significant heating of the ions is observed in the region of steepest gradients. For a reasonable estimate of electron temperature, the relative velocity of ions on either side of the front modestly exceeds the local sound speed (Mach number $M \geq 1$). This indicates that by sculpting steep density gradients, it is possible to create the conditions for shock formation, or very close to it, opening a new avenue of research for ultracold neutral plasmas.

© 2024 Author(s). All article content, except where otherwise noted, is licensed under a Creative Commons Attribution (CC BY) license (<https://creativecommons.org/licenses/by/4.0/>). <https://doi.org/10.1063/5.0237455>

02 May 2025 02:49:37

I. INTRODUCTION

A shockwave in a plasma is an abrupt jump in pressure, temperature, and density across a narrow front that propagates through the plasma.¹ Shocks can form when a driver moves through a plasma or a population of particles moves through a background plasma² at relative speeds that exceed the speed of sound. Ordinary waves can develop into shockwaves through wave steepening, in which nonlinear propagation effects lead to a steepening of leading density gradients.³ Plasma shockwaves are observed in many settings, such as laser-induced plasmas,⁴ supernova remnants,⁵ and the solar wind.⁶

In this paper, we present experimental observations of wave steepening and signatures of shock formation during the expansion of ultracold neutral plasmas (UNPs). UNPs are created by photoionizing laser cooled atoms^{7–9} or cold molecules in a supersonic expansion¹⁰ near the ionization threshold. They have been used to study many different plasma phenomena, such as plasma waves,^{11–14} streaming plasmas,¹⁵ three-body recombination,^{16,17} instabilities,¹⁸ and equilibration and transport in the strongly coupled regime.^{19–21} The expansion into surrounding vacuum of a UNP with an initial Gaussian density distribution has been studied extensively,^{11,22–28} including expansion in a uniform magnetic field.^{29,30} Recently, expansion of UNPs with an initial density distribution that decays exponentially with distance from

the plasma center was characterized experimentally in a field-free configuration³¹ and in a quadrupole magnetic field.³² Molecular dynamics simulations were presented for each case.^{33,34}

Since UNPs were first created,⁷ the development of shockwaves in this extreme environment has been of interest. Early fluid²² and hybrid molecular dynamics²³ models indicated shockwave formation in the low-density outer regions of expanding plasmas with an initial Gaussian density distribution. Experiments failed to detect such features within the limit of experimental sensitivity.²⁷ It has also been predicted that shocks develop in UNPs with non-Maxwellian electrons.³⁵ More recent molecular dynamics simulations of a Gaussian, quasi-neutral ultracold plasma showed that significant escape of electrons from the outer regions of the plasma and resulting non-neutrality can give rise to shock-like features.³³

Early numerical work by Sack and Schamel³⁶ in a very different context than UNPs, showed that expansion into vacuum of a plasma with an initial step-function density distribution yields wave-steepening and formation of a sharp density peak and shock structure. More recent work³⁷ shows that sharp fronts persist during the plasma expansion and points out the role of charge separation. Following this line of reasoning, the possibility of forming shocks in UNPs sculpted to have initial density distributions with steep density features

deviating from an ideal Gaussian has been discussed in multiple contexts.^{13–15,38} Experimental realizations produced streaming populations of UNPs, displaying a crossover from hydrodynamic^{13,14,39} to kinetic behavior¹⁵ with increasing initial density gradients and resulting relative velocities, but signatures of shock formation were not observed. A hydrodynamic model of colliding ultracold neutral molecular plasmas also predicted the formation of shocks.⁴⁰ While not in the UNP context, shockwaves have been seen in the Coulomb explosion of a cold, pure-ion, non-neutral plasma created by photo-excitation well above the ionization threshold such that electrons escape the system.⁴¹

We observe that the shape of the initial density distribution of a UNP largely determines the character of the plasma expansion when magnetic fields are negligible.³¹ Plasmas with a Gaussian-shaped initial density distribution, which are well-studied experimentally, expand self-similarly²⁷ and do not display detectable signatures of wave-steepening and shock formation. As shown in this study, however, plasmas formed with a more sharply peaked distribution that decays exponentially in space^{31,32} yield more complex dynamics, and after significant expansion, they display many of the traits that characterize the formation of shocks.

II. EXPERIMENTAL METHODS

We create UNPs from strontium atoms that are first laser cooled and trapped in a magneto-optical trap (MOT)⁴² operating on the $^1S_0-^1P_1$ principal transition at 461 nm. The MOT uses a quadrupole magnetic field produced by two coils in an anti-Helmholtz configuration. Figure 1 depicts the strontium atom level diagram and relevant decay paths. One in 2×10^4 atoms excited to the 1P_1 state by the cooling laser will decay into the 1D_2 state,⁴³ after which the atom will return to the ground 1S_0 state via the 3P_1 state or decay to the metastable 3P_2 state, with a 2:1 ratio.⁴⁴ A fraction of the atoms that decay into the 3P_2 state are trapped in a purely magnetic trap formed by the interaction of the atom's electronic spin with the quadrupole field of the MOT.⁴⁵ The resulting trapping potential yields an atomic density distribution that exponentially decays from the center of the trap, which is inherited by the plasma and is given by

$$n(\vec{r}) = n_0 \exp \left[-\frac{\sqrt{x^2 + (y^2 + z^2)/4\eta^2}}{\alpha} \right], \quad (1)$$

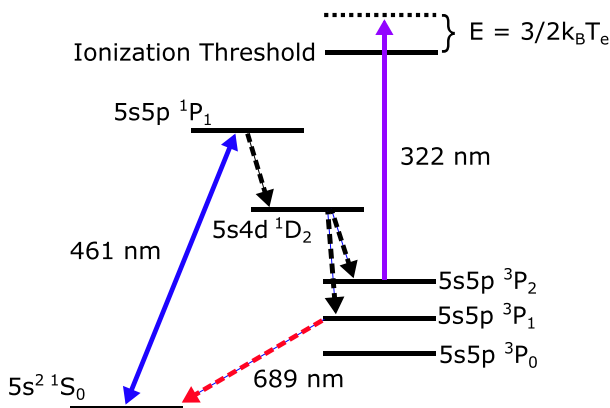


FIG. 1. Levels and transitions for laser cooling of strontium atoms, trapping in a purely magnetic trap, and subsequent photoionization to form a UNP.

where $\alpha = 3k_B T / (8\mu_B \partial B / \partial x)$ denotes the magnetic moment μ_B , gradient of the field along the symmetry axis is denoted by $\partial B / \partial x$, Boltzmann constant is denoted by k_B , and atom temperature is denoted by T . $\eta = 1$ for an equilibrated atomic sample, but we observe that the plasma density is the best fit with $\eta = 0.79$, indicating a lack of thermal equilibrium in the atoms that does not affect the conclusion of the present studies. In this experiment, $\alpha = 0.47$ mm.

After the magnetic trap is loaded with about 10^8 atoms, the cooling laser beams and the magnetic field are turned off. A 10 ns pulse of 322 nm light photoionizes the cloud of strontium atoms forming a plasma. The electron temperature is set by how far above the ionization threshold the 322-nm beam is detuned,⁸ as illustrated in Fig. 1. Experiments reported here were performed at electron temperatures ($T_e = 160$ K) high enough to avoid the effects of three body recombination, which increases at lower temperatures.¹¹

The early stages of UNP equilibration are described in Ref. 8. After photoionization, electrons equilibrate in the first few hundred nanoseconds. On the timescale of the ion plasma oscillation of about 1 μ s, the ions undergo disorder-induced heating (DIH)^{46,47} to a temperature of $T_i \approx e^2 / (12\pi\epsilon_0 a k_B) \approx 1$ K depending on the density, where e is the elementary charge, ϵ_0 is the vacuum permittivity, k_B is the Boltzmann constant, and $a = [3/(4\pi n_i)]^{1/3}$ is the Wigner-Seitz radius, and n_i is the ion density. Following intraspecies equilibration, the plasma expands into the surrounding vacuum. At an adjustable time after plasma creation, the Sr^+ ions are imaged using laser-induced fluorescence (LIF) on the $^2S_{1/2}-^2P_{1/2}$ transition at 422 nm.⁴⁸ Ions are excited with a thin (1 mm) sheet of laser light illuminating the central plane of the plasma. LIF emitted perpendicular to the light sheet is imaged onto an intensified charge coupled device (CCD) camera using a 1:1 optical relay with a resolution of 0.1 mm.

III. RESULTS

A. Plasma expansion and wave steepening

Figure 2(a) shows a false-color image of the density profile of a UNP 0.3 μ s after plasma formation, which is close to the initial plasma density distribution. The image is of the plane illuminated by the LIF laser, passing through the center of the plasma along the axis of cylindrical symmetry of the initial atomic density distribution.

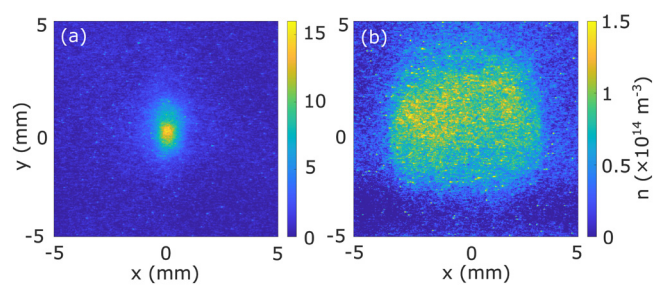


FIG. 2. False color images of the density in a cut through the plasma center. (a) 0.3 μ s after plasma creation. Tighter confinement along the x -axis of the atoms, and the resulting plasma creates a larger density gradient and hydrodynamic pressure, driving expansion along that axis. (b) 12 μ s after plasma creation. The aspect ratio of the plasma has inverted, and sharp transitions in the density are visible at the leading edge of expansion along the x -axis, suggesting wave steepening and shock formation.

UNP expansion is driven predominantly by the electron thermal pressure gradient. A hydrodynamic description yields the local acceleration given by Laha *et al.*²⁷

$$\dot{\vec{u}} = -\frac{k_B T_e}{m_i} \frac{\nabla n}{n}, \quad (2)$$

where u is the bulk plasma velocity, m_i is the mass of a strontium ion, T_e is the electron temperature, and n is the number density. This expression assumes quasi-neutrality, $n_i = n_e = n$, which is typically a good approximation for UNPs and holds when the electron temperature is low enough for the Debye length to be much less than the spatial scale for density variation in the plasma.⁸ The quasi-neutral approximation does not imply that the mean electric field vanishes in the plasma, as discussed in Ref. 8, and describing the expansion as resulting from the mean electric field provides an equivalent explanation. The Debye length for the peak density ($n = 15 \times 10^{14} \text{ m}^{-3}$ and $T_e = 160 \text{ K}$) is $23 \mu\text{m}$.

The steepest plasma gradients are along the x -axis [see Eq. (1)], producing the highest plasma acceleration along this axis and an inversion of the aspect ratio during the expansion as shown in the image taken at $12 \mu\text{s}$ in Fig. 2(b). Sharp transitions in the density are visible at the edges of the plasma experiencing the fastest expansion. We focus on the evolution of the density along the x -axis to look for signatures of wave steepening and shock formation.

A transect of the initial density at $y \approx 0$ is shown in Fig. 3. To fit the data, the 2D exponential [Eq. (1)] is averaged over a width in the z -axis corresponding to the thickness of the LIF light sheet. This produces a slight rounding of the peak. The overall match to the data are good, although there is some excess plasma in the regions of approximately $1 < |x| < 3 \text{ mm}$. This pedestal may contribute to wave steepening as it creates a region of lower $\nabla n/n$ and therefore lower initial acceleration velocity [Eq. (2)].

For an exponential density distribution, the hydrodynamic expression for acceleration [Eq. (2)] yields a step function, uniform on either side of the plasma, but with opposite signs. This would initially give rise to a velocity profile that is also a step function. The evolution is more complex than this simple picture because of initial deviations from a perfect exponential and the density distribution quickly evolves away from an exponential.

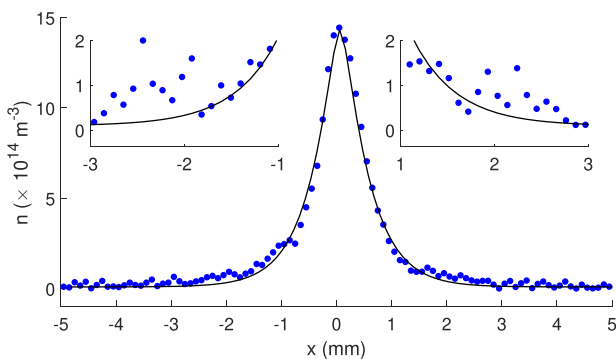


FIG. 3. Initial density along the x -axis at $y \approx z \approx 0$ from the image in Fig. 2(a) and a transect of a 2D exponential fit.

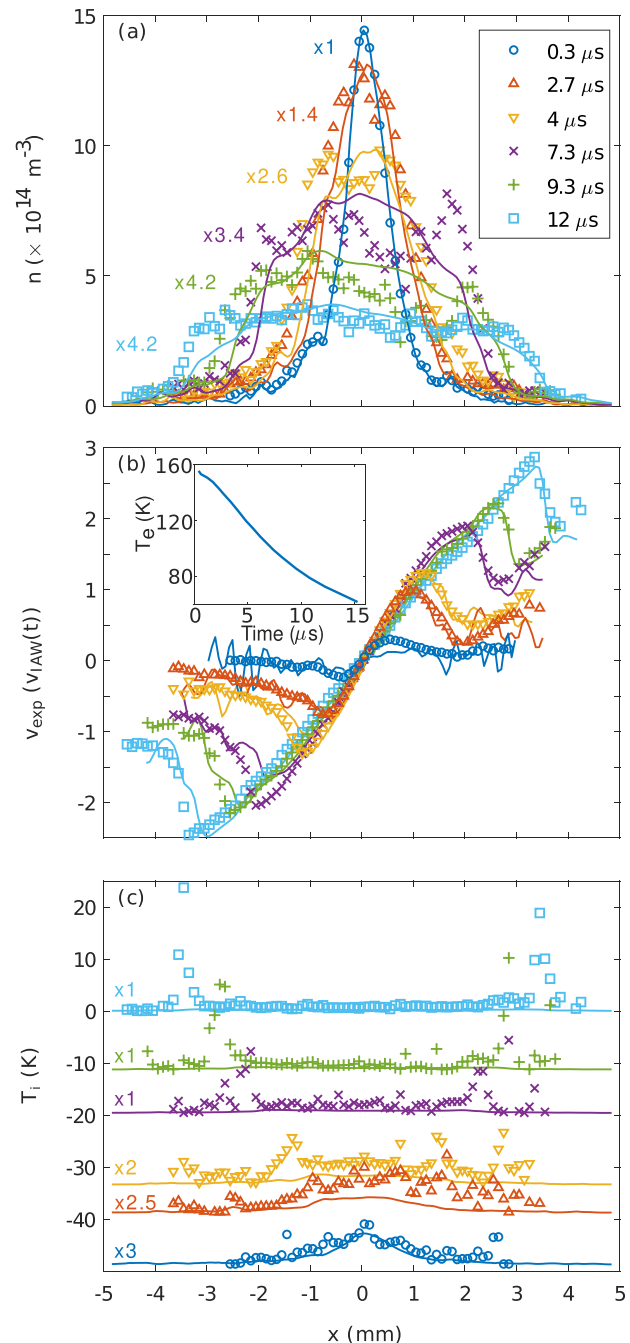


FIG. 4. Wave steepening during plasma expansion. Symbols are experimental data, and solid lines are results of a fluid simulation described in the text. (a) Density transects along x -axis for $y \approx z \approx 0$. (b) Velocity transects scaled by the ion acoustic wave speed ($v_{IAW} = 128, 120, 115, 101, 94$, and 86 m/s in order of increasing time). (c) Ion temperature transects for different times in the plasma expansion. T_i is offset by $-48.8, -38.8, -33.3, -19.6, -11.3$, and 0 K in order of increasing time. The offset is for clarity and is proportional to time to show the front propagation velocity. The calculated electron temperature, T_e (K), with respect to time is included as an inset in (b). Data and simulations are multiplied by the factors indicated in the figure to improve visibility.

Figure 4 shows transects of the experimentally measured plasma density (a), bulk velocity (b), and ion temperature (c) along the x -axis at various times after photoionization, compared to fluid simulations produced by SPRUCE, a multipurpose fluid code under development in the Solar Physics Research Group at Rice University.⁴⁹

The density [Fig. 4(a)] becomes flat in the center within the first few microseconds of evolution. As time progresses, the size of the central region of flat plasma density increases as the overall plasma expands and the peak density decreases. The leading edge of the plasma expansion accelerates with time as electron thermal energy is converted into directed kinetic energy of the ion expansion.¹¹

The expansion for the exponential plasma is clearly not self-similar. It is instructive to contrast it with the expansion of a spherical Gaussian density distribution^{27,31} given by $n = n_0 \exp(-r^2/2\sigma_0^2)$, for which the hydrodynamic force [Eq. (2)] yields an acceleration that increases linearly from zero at the plasma center. This yields a hydrodynamic velocity of $v = \gamma(t)r$ that increases linearly with distance from the plasma center and initially increases with time, resulting in a self-similar expansion, $\sigma_0 \rightarrow \sigma(t)$. Both $\gamma(t)$ and $\sigma(t)$ can be expressed analytically.^{8,27}

For the exponential plasma, the acceleration is initially much larger near the center than for a Gaussian plasma of comparable size and electron temperature, but the acceleration of the Gaussian plasma will be greater at large radial distance. An exponential density is therefore susceptible to the development of a velocity distribution that displays extrema away from the plasma center, as shown in Fig. 4(b). For the earliest time point, the sharply peaked center of the plasma may experience significant non-neutrality in a region on the order of the Debye length, which is $23 \mu\text{m}$ for the peak density. This may create a local Coulomb explosion that also contributes to the acceleration of ions from the central region.³¹

The bulk velocity in the flat central region of the exponential plasma is well-approximated by the linear relationship $v = x/t$ after the first few microseconds, indicating that plasma in this region quickly evolves to a state of expansion with vanishing acceleration, as expected for a flat density [Eq. (2)]. Note that Fig. 4(b) shows the velocity scaled by the ion acoustic wave velocity, which will be discussed in detail as follows and is given for each trace in the caption of the figure. The largest observed peak expansion velocities are $\sim 200 \text{ m/s}$ at $7 \mu\text{s}$.

The peaks of the ion velocity for positive and negative x precisely correspond to the edges of the central density plateau. In the velocity profiles, it is evident that in the range $0.3 - 7.3 \mu\text{s}$, higher-velocity plasma is overtaking lower-velocity plasma in front of it yielding wave steepening. By $\sim 7 \mu\text{s}$, this creates well-defined high-density, high-velocity fronts that propagate through the low-density, low-velocity plasma in front of them, with a large jump in density and velocity across the front.

At $12 \mu\text{s}$, the velocity peaks and gradients are extremely sharp, with a length scale for the front (from 75% to 25% of peak density) of 0.4 mm , much smaller than the several-millimeter scale of the overall plasma. The jump in velocity is over 100 m/s . The spatial overlap of the sharp density and velocity features is clearly seen in the expanded views shown in Fig. 5.

The experimental and simulation results agree reasonably well. The simulation treats the plasma as an ideal quasi-neutral fluid in two dimensions with one continuity and momentum equation and

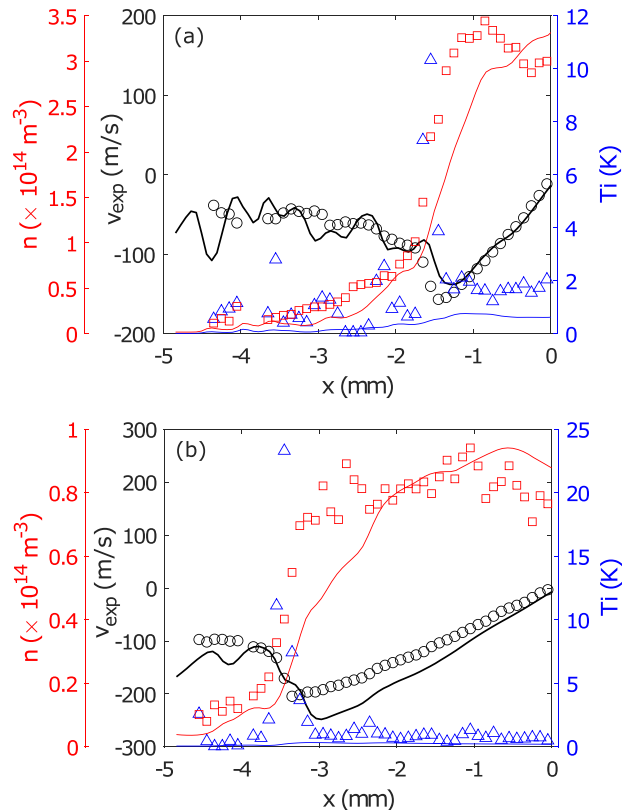


FIG. 5. Transects for the plasma expansion velocity (v), density (n), and ion temperature (T_i) for the left half of the plasma at (a) $5.3 \mu\text{s}$ and (b) $12.0 \mu\text{s}$ expansion times. The principal features in each trace overlap spatially. Solid lines are numerical simulations.

separate electron and ion energy equations. We equate the ambipolar electric field force term to the electron pressure gradient through $en_i E \approx \nabla P_e$. The fluid equations are solved on a uniform Cartesian grid using Barton's method for monotonic transport to compute transport derivatives, second-order central finite differences for all other derivatives, and a second-order Runge-Kutta time integration scheme.⁴⁹ Barton's method is a simple, yet robust, method of differentiation for discontinuous fluid problems that result in shock conditions without post-shock oscillations present in other methods.⁵⁰ Open boundary conditions are implemented by choosing a large simulation domain $|x|, |y| < 1.2 \text{ cm}$ and limiting spatial derivatives at the boundary through the use of two ghost cells, which copy the fluid characteristics of the nearest interior cell.

The plasma density is initialized on the domain by interpolating the density distribution shown in Fig. 2 for distance from the center $|r| < 5 \text{ cm}$ and filling all cells exterior to this radius with an exponential fit to the distribution in Fig. 2 superimposed on a small uniform background (10^{-4} of peak density) to avoid simulation instability at vanishing density. The initial electron temperature is set to 160 K to match the energy expected from the detuning of the ionizing laser above resonance. The ion temperature profile is set to the initial measured value, after disorder-induced heating.

Electron thermal energy redistributes rapidly across the plasma because of the large electron mean free path (MFP) ($\lambda_e \gg \alpha$). To capture this behavior, the electrons are held in global thermal equilibrium by replacing the electron temperature distribution with a uniform value \bar{T}_e following each update to the fluid variables,

$$\bar{T}_e = \frac{1}{N} \int n T_e(x, y) dx dy, \quad (3)$$

where $N = \int n dx dy$. Solving the electron energy equation and redistributing the thermal energy in this way allows for the capture of expansion-induced cooling while conserving thermal energy and avoiding unphysical temperature gradients.

The validity of this quasi-kinetic treatment of the electrons, where the electrons are globally hydrodynamic but locally kinetic, has been demonstrated for UNPs with a variety of initial density distributions such as a spherically symmetric Gaussian density distribution imprinted with planar ion holes and periodic perturbations that excite ion acoustic waves.⁴⁹ The simulations in two dimensions accurately capture the key elements of the plasma expansion dynamics. The pressure gradients that drive plasma acceleration are identical in each case as is the resulting expansion-induced cooling for thermal energy density, $e = P/(\gamma - 1)$, where P is the plasma pressure, which is dominated by the electrons. $\gamma = 2$ is the two-dimensional adiabatic index used in the simulations. Likewise, the plasma sound speed is identical in each case due to its independence of the adiabatic index under locally kinetic conditions where $T_e \gg T_i$.

One consequence of simulating in two dimensions is the plasma is effectively treated as uniform in the z direction. Thus, the simulations will neglect ion flux out of the central plane, causing the absolute density to be higher in the simulations. The lack of self-similarity in plasma expansion can result in differences in the evolution of the density distribution. However, the absolute density does not play a role in driving the plasma expansion or the sound speed. The agreement between experiment and simulation for the renormalized density profile and absolute velocity distribution gives confidence that the electron temperature predicted by the simulation is a reasonable estimate of the actual electron temperature. We use this electron temperature to calculate the ion acoustic wave speed for Fig. 4(b).

B. Mach number

In addition to jumps in velocity and density over a small length scale, a shockwave displays a relative flow velocity that exceeds the local sound speed so that information of the oncoming shock cannot propagate before it. This is characterized with a Mach number $M > 1$. We define M for our system as

$$M = \frac{v_{rel}}{v_s}, \quad (4)$$

where v_{rel} is the relative velocity between the plasma populations on either side of the front, and v_s is the sound speed in the plasma. For an unmagnetized plasma, the sound speed is the ion acoustic wave speed for kinetic electrons and hydrodynamic ions, which is given by

$$v_{IAW} = \sqrt{\frac{k_B}{m_i} (T_e + \gamma_i T_i)}, \quad (5)$$

where k_B is the Boltzmann constant, m_i is the ion mass, T_e is the electron temperature, and T_i is the ion temperature. γ_i is the adiabatic index for the ions and is 5/3 because acoustic wave compression is isentropic.

Knowledge of the electron temperature is essential to estimate the ion acoustic wave speed. We are unable to directly measure the electron temperature; however, the initial electron temperature is set by the ionization laser detuning above the threshold^{7,8,26} ($T_e(0) = 160$ K for the data discussed here). We can also reliably assume global thermal equilibrium for the electrons because the MFP is on the order of the size of the plasma, and the collision time is short compared to the plasma expansion time. Initially, for 160 K and a density of $15 \times 10^{14} \text{ m}^{-3}$, the MFP for an electron moving with the thermal velocity is 2.4 mm.

We compare three different estimates of the electron temperature and ion acoustic wave speed for each time point during the plasma expansion. An upper bound for both is given by $T_e = T_e(0)$, which neglects adiabatic cooling of the electrons during the plasma expansion. This yields a lower limit on the Mach number. Alternatively, an approximate value of $T_e(t)$ can be obtained from a simple estimate of the volume V of the plasma at each time derived from the plasma images assuming cylindrical symmetry and adiabatic cooling of the electrons according to $T_e V^{2/3} = \text{constant}$.²³ Finally, from the 2D fluid simulation, we extract the simulated $T_e(t)$, which we take as our most reliable value. Figure 4(b) shows the velocity transects scaled by the ion acoustic wave speed using $T_e(t)$ from the hydrodynamic simulation. For calculating v_{IAW} , the ion temperature is negligible.

Figure 6 shows the Mach number as a function of time for the left side of the plasma ($x < 0$). The relative velocity is taken as the difference between the peak velocity and the mean velocity in the region of relatively constant velocity near the edge of the plasma. Initially, $M < 1$, but for expansion times greater than $\sim 7 \mu\text{s}$, the Mach number slightly exceeds unity (or comes very close to unity when using the lower bound). 7.3 μs is also the time where the velocity profile

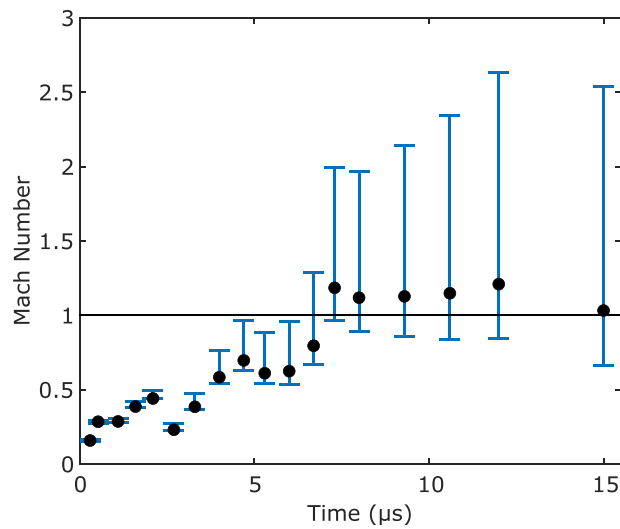


FIG. 6. Mach number evolution for the plasma front for $x < 0$. Upper and lower bounds are described in the text.

develops a sharp kink at the peak [Fig. 4(b)], further suggesting the formation of a shockwave.

C. Localized heating

The plasma also displays localized heating in the ion temperature where the density and velocity gradients are highest, as shown by Figs. 4(c) and 5. Initially (e.g., for plasma evolution time $t = 0.3 \mu\text{s}$), the ion temperature is relatively smooth. Disorder-induced heating (DIH)^{46,47} should yield a density-dependent temperature, with the highest value in the plasma center of 1.2 K for density of $14 \times 10^{14} \text{ m}^{-3}$. The observed temperature is higher (2.6 K in the center). This may arise from kinetic effects and initial non-neutrality in the region of very high density gradient in the plasma center.³¹ The center of the plasma adiabatically cools throughout the plasma expansion, as expected.

As wave steepening develops in the plasma, increases in the ion temperature form and grow at the density and velocity jump. This behavior becomes prominent at $7.3 \mu\text{s}$ in Fig. 4(c). Ion temperatures in the front exceed 10 K where the density and velocity jumps are greatest. Plotting the density, velocity, and temperature transects on the same plot, as shown in Fig. 5 for $7.3 \mu\text{s}$, shows the overlap of the temperature features with the front. The numerical simulation only displays a small temperature rise in the region of the front, most clearly seen in Fig. 5(a). This suggests that the temperature spikes arise from kinetic effects, which are not included in the simulation.

It is important to consider that an overestimation in the ion temperature could arise from artificial spectral broadening introduced by the finite resolution of the imaging system and analysis. This is a concern because of the large velocity gradient at the location of the temperature spike, and because we measure the spectra over a finite region size (0.1 mm).

The magnitude of the largest velocity gradient in the data is $3.6 \times 10^5 \text{ s}^{-1}$ at $12 \mu\text{s}$ [Fig. 4(b)]. For a 0.1 mm region, this introduces a velocity spread of $\Delta v = 36 \text{ m/s}$. A simple upper bound on the increase in the temperature extracted from spectral analysis is $\Delta T \approx m\Delta v^2/2k_B = 7 \text{ K}$, which does not account for the observed temperature in excess of 20 K.

To better estimate the spectral broadening due to the velocity gradient, we developed a simulation that divides each 0.1 mm region into smaller subregions in which the velocity spread can be ignored. The simulation creates spectra for each subregion and then adds them together to create the simulated spectrum for the original 0.1 mm region. Simulated spectra are then analyzed in the same way as the experimental data and yield only about 2 K of increase in the measured temperature due to the finite region size for the largest velocity gradients.

IV. ION MEAN FREE PATH

As discussed earlier, the electron MFP is on the order of the plasma size, and the collision time is short compared to the timescale for plasma expansion. This allows us to assume global thermal equilibrium for the electrons. The situation for ions is more complex. The MFP for an ion moving at the thermal velocity for 1 K is $28 \mu\text{m}$ for a typical density of $1 \times 10^{14} \text{ m}^{-3}$. This is small relative to the size of the plasma, which is consistent with the lack of global thermal equilibrium observed in the system [Fig. 4(c)]. In regions away from the expanding

fronts, the ions quickly establish local thermal equilibrium because the collision time and the timescale for DIH is $\sim 1 \mu\text{s}$.⁴⁷

At the front, however, the large relative velocities of ions in the low density and high density sides of about 100 m/s yield much longer MFPs. For the typical density on the high density side of $1 \times 10^{14} \text{ m}^{-3}$, the MFP is 6 mm, which is very large compared to the size of the shock front. Therefore, we expect a significant fraction of the population of low density ions in front of the shock to penetrate into the high density region overtaking it. A detailed description of this process would require a calculation of the stopping power of the ions, including possible effects from strong coupling,⁵¹ which is beyond the scope of this paper. We expect that the population of ions in the high density region expanding outward is in local thermal equilibrium with itself due to the high collisionality. Any streaming population is too small to detect relative to the high density population. LIF spectra for plasma in the transition region are fit well with a line shape that assumes local thermal equilibrium.

V. CONCLUSION

We have presented evidence of wave steepening and signatures of shock formation in UNPs formed with an initially sharply peaked density distribution. As the plasma expands, sharp transitions in density and velocity form at expanding fronts that also display localized ion heating where plasma from the inner, high-density region overtakes outer, lower-density plasma. Using the electron temperature taken from a fluid simulation, Mach numbers slightly greater than unity are observed. This work establishes that conditions for shock formation, or near to it, can be obtained in UNPs with sculpted density distributions.

These data present a rich challenge for testing hydrodynamic and kinetic theories and for searching for effects of strong coupling on viscosity through damping of the shock features. Future work can explore the variation of the observed features with plasma density and initial electron temperature. Expanding the field of view for plasma imaging would enable exploration of whether wave steepening continues or is eventually balanced by dissipation.

ACKNOWLEDGMENTS

This work was supported by the NSF/DOE Partnership in Basic Plasma Science and Engineering under Award No. 2107709, the National Science Foundation Graduate Research Fellowship Program under Grant No. 1842494, and the NSF-CAREER award AGS-1450230. Any opinions, findings, and conclusions or recommendations expressed in this material are those of the authors and do not necessarily reflect the views of the National Science Foundation.

AUTHOR DECLARATIONS

Conflict of Interest

The authors have no conflicts to disclose.

Author Contributions

M. K. Warrens: Conceptualization (lead); Data curation (lead); Formal analysis (lead); Investigation (lead); Methodology (lead); Software (equal); Supervision (supporting); Validation (lead); Visualization (lead); Writing – original draft (lead); Writing – review

& editing (lead). **N. P. Inman:** Data curation (supporting); Investigation (supporting); Software (supporting); Validation (supporting); Visualization (supporting); Writing – original draft (supporting); Writing – review & editing (supporting). **G. M. Gorman:** Conceptualization (equal); Formal analysis (equal); Investigation (equal); Methodology (equal); Software (lead); Supervision (equal); Visualization (equal); Writing – original draft (equal); Writing – review & editing (equal). **B. T. Husick:** Investigation (supporting); Software (supporting); Visualization (supporting); Writing – review & editing (supporting). **S. J. Bradshaw:** Conceptualization (equal); Funding acquisition (lead); Investigation (equal); Methodology (equal); Project administration (equal); Resources (lead); Software (equal); Supervision (equal); Writing – review & editing (equal). **T. C. Killian:** Conceptualization (lead); Formal analysis (equal); Funding acquisition (lead); Investigation (equal); Methodology (equal); Project administration (lead); Resources (lead); Supervision (equal); Writing – original draft (equal); Writing – review & editing (equal).

DATA AVAILABILITY

The data that support the finding of this study are available from the corresponding author upon reasonable request.

REFERENCES

- ¹L. D. Landau and E. M. Lifshits, *Fluid Mechanics* (Pergamon Press, Elmsford, NY, 1987).
- ²A. Balogh and R. A. Treumann, *Physics of Collisionless Shocks* (Springer, New York, 2013).
- ³G. B. Whitham, *Linear and Nonlinear Waves*, 1st ed. (Wiley-Interscience, New York, 1999).
- ⁴B. Campanella, S. Legnaioli, S. Pagnotta, F. Poggialini, and V. Palleschi, “Shock waves in laser-induced plasmas,” *Atoms* **7**, 57 (2019).
- ⁵R. A. Treumann, “Fundamentals of collisionless shocks for astrophysical application, I. non-relativistic shocks,” *Astron. Astrophys. Rev.* **17**, 409 (2009).
- ⁶R. B. Scott, S. J. Bradshaw, and M. G. Linton, “The dynamic evolution of solar wind streams following interchange reconnection,” *Astrophys. J.* **933**, 72 (2022).
- ⁷T. C. Killian, S. Kulin, S. D. Bergeson, L. A. Orozco, C. Orzel, and S. L. Rolston, “Creation of an ultracold neutral plasma,” *Phys. Rev. Lett.* **83**, 4776 (1999).
- ⁸T. C. Killian, T. Pattard, T. Pohl, and J. M. Rost, “Ultracold neutral plasmas,” *Phys. Rep.* **449**, 77 (2007).
- ⁹T. Kroker, M. Großmann, K. Sengstock, M. Drescher, P. Wessels-Staarmann, and J. Simonet, “Ultrafast electron cooling in an expanding ultracold plasma,” *Nat. Comm.* **12**, 596 (2021).
- ¹⁰J. P. Morrison, C. J. Rennick, J. S. Keller, and E. R. Grant, “Evolution from a molecular Rydberg gas to an ultracold plasma in a seeded supersonic expansion of NO,” *Phys. Rev. Lett.* **101**, 205005 (2008).
- ¹¹S. Kulin, T. C. Killian, S. D. Bergeson, and S. L. Rolston, “Plasma oscillations and expansion of an ultracold neutral plasma,” *Phys. Rev. Lett.* **85**, 318 (2000).
- ¹²S. D. Bergeson and R. L. Spencer, “Neutral-plasma oscillations at zero temperature,” *Phys. Rev. E* **67**, 026414 (2003).
- ¹³J. Castro, P. McQuillen, and T. C. Killian, “Ion acoustic waves in ultracold neutral plasmas,” *Phys. Rev. Lett.* **105**, 065004 (2010).
- ¹⁴P. McQuillen, J. Castro, T. Strickler, S. J. Bradshaw, and T. C. Killian, “Ion holes in the hydrodynamic regime in ultracold neutral plasmas,” *Phys. Plasmas* **20**, 043516 (2013).
- ¹⁵P. McQuillen, J. Castro, S. J. Bradshaw, and T. C. Killian, “Emergence of kinetic behavior in streaming ultracold neutral plasmas,” *Phys. Plasmas* **22**, 043514 (2015a).
- ¹⁶T. C. Killian, M. J. Lim, S. Kulin, R. Dumke, S. D. Bergeson, and S. L. Rolston, “Formation of Rydberg atoms in an expanding ultracold neutral plasma,” *Phys. Rev. Lett.* **86**, 3759 (2001).
- ¹⁷R. S. Fletcher, X. L. Zhang, and S. L. Rolston, “Using three-body recombination to extract electron temperatures of ultracold plasmas,” *Phys. Rev. Lett.* **99**, 145001 (2007).
- ¹⁸X. L. Zhang, R. S. Fletcher, and S. L. Rolston, “Observation of an ultracold plasma instability,” *Phys. Rev. Lett.* **101**, 195002 (2008).
- ¹⁹M. S. Murillo, “Using fermi statistics to create strongly coupled ion plasmas in atom traps,” *Phys. Rev. Lett.* **87**, 115003 (2001).
- ²⁰G. Bannasch, J. Castro, P. McQuillen, T. Pohl, and T. C. Killian, “Velocity relaxation in a strongly coupled plasma,” *Phys. Rev. Lett.* **109**, 185008 (2012).
- ²¹T. Sprenkle, A. Dodson, E. McKnight, R. Spencer, S. Bergeson, A. Diaw, and M. S. Murillo, “Ion friction at small values of the coulomb logarithm,” *Phys. Rev. E* **99**, 053206 (2019).
- ²²F. Robicheaux and J. D. Hanson, “Simulated expansion of an ultra-cold, neutral plasma,” *Phys. Plasmas* **10**, 2217 (2003).
- ²³T. Pohl, T. Pattard, and J. M. Rost, “Kinetic modeling and molecular dynamics simulation of ultracold neutral plasmas including ionic correlations,” *Phys. Rev. A* **70**, 033416 (2004a).
- ²⁴T. Pohl, T. Pattard, and J. M. Rost, “Coulomb crystallization in expanding laser-cooled neutral plasmas,” *Phys. Rev. Lett.* **92**, 155003 (2004b).
- ²⁵E. A. Cummings, J. E. Daily, D. S. Durfee, and S. D. Bergeson, “Flourescence measurements of expanding strongly coupled neutral plasmas,” *Phys. Plasmas* **12**, 123501 (2005).
- ²⁶P. Gupta, S. Laha, C. E. Simien, H. Gao, J. Castro, T. C. Killian, and T. Pohl, “Electron-temperature evolution in expanding ultracold neutral plasmas,” *Phys. Rev. Lett.* **99**, 75005 (2007).
- ²⁷S. Laha, P. Gupta, C. E. Simien, H. Gao, J. Castro, and T. C. Killian, “Experimental realization of an exact solution to the Vlasov equations for an expanding plasma,” *Phys. Rev. Lett.* **99**, 155001 (2007).
- ²⁸P. McQuillen, T. Strickler, T. Langin, and T. C. Killian, “Experimental measurement of self-diffusion in a strongly coupled plasma,” *Phys. Plasmas* **22**, 033513 (2015b).
- ²⁹X. L. Zhang, R. S. Fletcher, S. L. Rolston, P. N. Guzdar, and M. Swisdak, “Ultracold plasma expansion in a magnetic field,” *Phys. Rev. Lett.* **100**, 235002 (2008).
- ³⁰R. T. Sprenkle, S. D. Bergeson, L. G. Silvestri, and M. S. Murillo, “Ultracold neutral plasma expansion in a strong uniform magnetic field,” *Phys. Rev. E* **105**, 045201 (2022).
- ³¹M. K. Warrens, G. M. Gorman, S. J. Bradshaw, and T. C. Killian, “Expansion of ultracold neutral plasmas with exponentially decaying density distributions,” *Phys. Plasmas* **28**, 022110 (2021).
- ³²G. M. Gorman, M. K. Warrens, S. J. Bradshaw, and T. C. Killian, “Magnetic confinement of an ultracold neutral plasma,” *Phys. Rev. Lett.* **126**, 085002 (2021).
- ³³E. Vikhrov, S. Y. Bronin, B. B. Zelener, and B. V. Zelener, “Ion wave formation during ultracold plasma expansion,” *Phys. Rev. E* **104**, 015212 (2021).
- ³⁴S. Y. Bronin, E. V. Vikhrov, B. B. Zelener, and B. V. Zelener, “Ultracold plasma expansion in quadrupole magnetic field,” *Phys. Rev. E* **108**, 045209 (2023).
- ³⁵P. Shukla, W. M. Moslem, S. S. Duha, and A. A. Mamun, “Time evolution of cylindrical and spherical shock waves in an ultracold neutral plasma with non-Maxwellian electrons,” *Europhys. Lett.* **96**, 65002 (2011).
- ³⁶C. Sach and H. Schamel, “Evolution of a plasma expanding into vacuum,” *Plasma Phys. Controlled Fusion* **27**, 717 (1985).
- ³⁷P. Mora, “Plasma expansion into a vacuum,” *Phys. Rev. Lett.* **90**, 185002 (2003).
- ³⁸V. S. Dharodi and M. S. Murillo, “Sculpted ultracold neutral plasmas,” *Phys. Rev. E* **101**, 023207 (2020).
- ³⁹T. C. Killian, P. McQuillen, T. M. O’Neil, and J. Castro, “Creating and studying ion acoustic waves in ultracold neutral plasmas,” *Phys. Plasmas* **19**, 055701 (2012).
- ⁴⁰J. P. Morrison and E. R. Grant, “Dynamics of colliding ultracold plasmas,” *Phys. Rev. A* **91**, 023423 (2015).
- ⁴¹M. A. Viray, S. A. Miller, and G. Raithel, “Coulomb expansion of a cold non-neutral rubidium plasma,” *Phys. Rev. A* **102**, 033303 (2020).
- ⁴²H. J. Metcalf and P. van der Straten, *Laser Cooling and Trapping* (Springer-Verlag, New York, 1999).
- ⁴³A. Cooper, J. P. Covey, I. S. Madjarov, S. G. Porsev, M. S. Safranova, and M. Endres, “Alkaline-earth atoms in optical tweezers,” *Phys. Rev. X* **8**, 041055 (2018).

⁴⁴X. Xu, T. H. Loftus, J. L. Hall, A. Gallagher, and J. Ye, "Cooling and trapping of atomic strontium," *J. Opt. Soc. Am. B* **20**, 968–976 (2003).

⁴⁵S. B. Nagel, C. E. Simien, S. Laha, P. Gupta, V. S. Ashoka, and T. C. Killian, "Magnetic trapping of metastable 3P_2 atomic strontium," *Phys. Rev. A* **67**, 011401(R (2003).

⁴⁶Y. C. Chen, C. E. Simien, S. Laha, P. Gupta, Y. N. Martinez, P. G. Mickelson, S. B. Nagel, and T. C. Killian, "Electron screening and kinetic-energy oscillations in a strongly coupled plasma," *Phys. Rev. Lett.* **93**, 265003 (2004).

⁴⁷T. K. Langin, T. Strickler, N. Maksimovic, P. McQuillen, T. Pohl, D. Vrinceanu, and T. C. Killian, "Demonstrating universal scaling for dynamics of Yukawa one-component plasmas after an interaction quench," *Phys. Rev. E* **93**, 023201 (2016).

⁴⁸J. Castro, H. Gao, and T. C. Killian, "Using sheet fluorescence to probe ion dynamics in an ultracold neutral plasma," *Plasma Phys. Controlled Fusion* **50**, 124011 (2008).

⁴⁹G. Szyplko, G. Gorman, and S. Bradshaw, "Modeling fluid evolution of interchange reconnection aftermath," in AAS/Solar Physics Division Meeting (2023) <https://baas.aas.org/pub/2023n7i107p04>.

⁵⁰J. Centrella and J. W. Wilson, "Planar numerical cosmology. ii. the difference equations and numerical tests," *Astrophys. J. Suppl. Ser.* **54**, 229–249 (1984).

⁵¹K. Morawetz and G. Röpke, "Stopping power in nonideal and strongly coupled plasmas," *Phys. Rev. E* **54**, 4134–4146 (1996).